

pubs.acs.org/ac Technical Note

Simultaneous Determination of Linear and Nonlinear Electrophoretic Mobilities of Cells and Microparticles

Sofia Antunez-Vela, Victor H. Perez-Gonzalez,* Adriana Coll De Peña, Cody J. Lentz, and Blanca H. Lapizco-Encinas*



Cite This: Anal. Chem. 2020, 92, 14885-14891



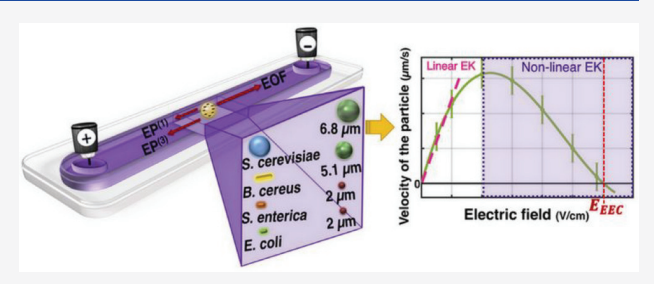
ACCESS

Metrics & More

Article Recommendations

s Supporting Information

ABSTRACT: Direct-current insulator-based electrokinetics (DC-iEK) is a branch of microfluidics that has demonstrated to be an attractive and efficient technique for manipulating micro- and nano- particles, including microorganisms. A unique feature of DC-iEK devices is that nonlinear EK effects are enhanced by the presence of regions of higher field intensity between the insulating structures. Accurate computational models, describing particle and cell behavior, are crucial to optimize the design and improve the performance of DC-iEK devices. The electrokinetic equilibrium condition ($E_{\rm EEC}$) is a recently introduced fundamental concept that



has radically shifted the perspective behind the analysis of particle manipulation in these microfluidic devices. The $E_{\rm EEC}$ takes into consideration previously neglected nonlinear effects on particle migration and indicates that these effects are central to control particle motion in DC-iEK devices. In this study, we present a simultaneous experimental characterization of linear and nonlinear electrokinetic (EK) parameters, that is, the electrophoretic mobility ($\mu_{\rm EP}^{(1)}$), the particle zeta potential ($\zeta_{\rm P}$), the $E_{\rm EEC}$, and the electrophoretic mobility of the second kind ($\mu_{\rm EP}^{(3)}$), for four types of polystyrene microparticles and four cell strains. For this, we studied the electromigration of polystyrene microparticles ranging in size from 2 to 6.8 μ m, three bacteria strains (B. cereus, E. coli, and S. enterica) and a yeast cell (S. cerevisiae), ranging in size from 1 to 6.3 μ m, in a polydimethylsiloxane (PDMS) microfluidic channel with a rectangular cross-section. The results illustrated that electrokinetic particle trapping can occur by linear and nonlinear electrophoresis and electroosmosis reaching an equilibrium, without the presence of insulating posts. The experimentally measured parameters reported herein will allow optimizing the design of future DC-iEK devices for a wide range of applications (e.g., to separate multiple kinds of particles and microorganisms) and for developing computational models that better represent reality.

he research and technological fields of analytical chemistry and bioanalysis require powerful particle manipulation techniques to perform efficient sample preparation protocols. These techniques must handle the complexity of the extensive realm of bioparticles, ranging in nature from macromolecules to parasites and in size from a couple of nm to several mm.¹⁻⁶ Microfluidic techniques have proven to be an attractive option for numerous bioanalytical applications due to the inherent benefits of working on the microscale (i.e., short response times, low sample volume requirement, and ease of integration with other processes).^{7,8} Furthermore, microfluidic devices have the ability to carry out single molecule⁹ and single cell analysis, 10,11 making them an excellent choice for sensing applications. Additionally, microfluidic techniques are making an important impact in developing point-of-care (POC) devices able to provide patients with rapid and accurate diagnostics, a critical necessity in low-income communities with no access to clinical analysis laboratories. 12,13 This basic need has become a strong driving force for the development of novel microfluidic techniques for bioparticle assessment, enrichment, and sensing. 14

Electrokinetics (EK) is one of the main pillars of microfluidics. In particular, direct current insulator-based EK (DC-iEK) microfluidic devices allow combining several mechanisms, that is, electrophoresis (EP), electroosmosis (EO), and dielectrophoresis (DEP), simultaneously for micro- and nanoparticle manipulation, including biological particles. Until recently, it was believed that the main force driving particle motion and allowing for particle manipulation in these devices was DEP; this belief was, in fact, so widely accepted that this research field was previously called "direct current insulator-based dielectrophoresis" (DC-iDEP). However, recently, Cardenas-Benitez et al. revealed that it is the balance between linear EO, linear EP, and nonlinear EP that leads to particle manipulation in these

Received: August 19, 2020 Accepted: October 18, 2020 Published: October 27, 2020





devices when stimulated with high-magnitude electric fields.¹⁷ This balance was defined as the electrokinetic equilibrium condition (E_{EEC}) , which considers previously neglected nonlinear effects on particle migration. Nonlinear EP (also known as EP of the second kind or EP⁽³⁾) had been extensively studied in colloid research. Nonetheless, except for a handful of studies focused on the electrokinetic response of particles stimulated with high electric fields, ^{20–22} EP⁽³⁾ had mostly been neglected in DC-iEK. Coll De Peña et al. 23,24 demonstrated the first applications of $E_{\rm EEC}$ and the theoretical framework developed by Cardenas-Benitez et al. 17 for the manipulation of several microorganisms in two different devices; Quevedo et al.²⁵ applied this framework to protein nanoparticles. These two recent applications further validate this novel approach to interpret DC-iEK experimental observations. Also, in a recent study, Tottori et al. 21 analyzed the electromigration and trapping of polystyrene and poly-(methyl methacrylate) (PMMA) submicron particles under high electric fields in a similar experimental setup to that used by Cardenas-Benitez et al., 17 exhibiting similar trends in their observations. The discovery of DEP not being the main force driving particle motion in insulator-based systems represents a major shift in the field of DC-EK-driven microfluidics, eliminating the use of correction factors in modeling (a previously widespread common practice). ²⁶ Furthermore, these recent studies also demonstrated that DEP only made a minor contribution to particle migration, since it only represented 0.89% to 5.85% of the EP⁽³⁾ velocity. 17,2

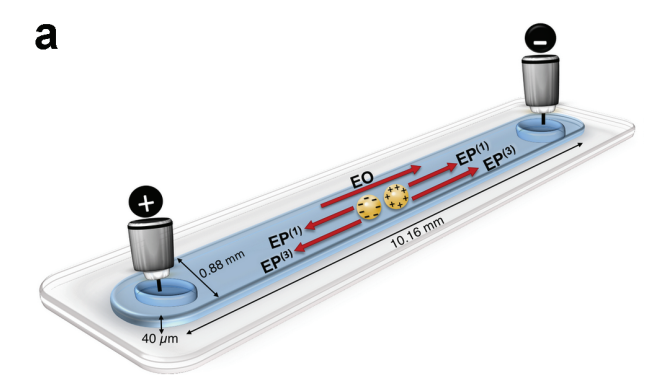
This study presents a methodology for simultaneously characterizing the linear and nonlinear EP mobilities of polystyrene microparticles and cells. A major and unique contribution of this work is the characterization of the EP(3) mobility of microparticles and cells. To the best of our knowledge, no previous reports exist in the literature for the EP⁽³⁾ mobility characterization of cells. To test the proposed methodology, four distinct types of polystyrene microparticles and four distinct types of cells were used in our experiments, which were conducted in polydimethylsiloxane (PDMS) microchannels with a constant rectangular cross section. The polystyrene microparticles ranged in sizes from 2.0 to 6.8 μ m. The cell strains studied were B. cereus, E. coli, S. enterica, and S. cerevisiae, ranging in size from 1 to 6.3 μ m. The results confirmed that linear and nonlinear EP balancing EOF are the dominant mechanisms driving particle manipulation under high electric fields and support the results from our previous studies. 17,23 The results illustrated that electrokinetic particle trapping can occur by linear and nonlinear electrophoresis and electroosmosis reaching an equilibrium, without the presence of insulating posts. These findings establish the importance of determining nonlinear mobility data for the design of effective microscale DC-iEK systems for the analysis and separation of particles and cells.

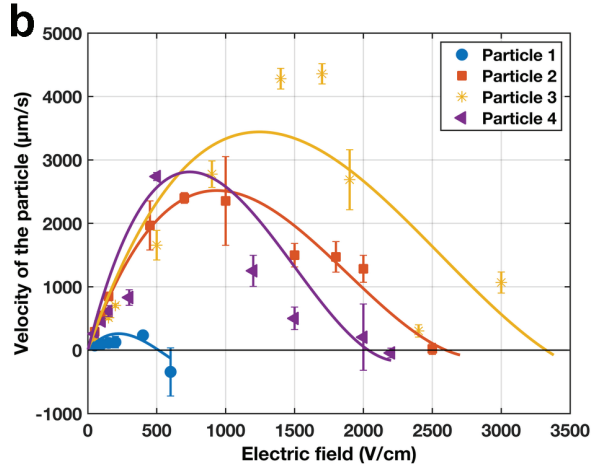
■ THEORY

In our system, the total particle velocity can be expressed as a function of three EK phenomena, as illustrated in Figure 1a for a negatively and a positively charged particle, respectively:

$$\mathbf{v}_{\mathrm{P}} = \mathbf{v}_{\mathrm{EO}} + \mathbf{v}_{\mathrm{EP}}^{(1)} + \mathbf{v}_{\mathrm{EP}}^{(3)} \tag{1}$$

where ${\bf v}_{EO}$, ${\bf v}_{EP}^{(1)}$, and ${\bf v}_{EP}^{(3)}$ are the velocities associated with EO, EP $^{(1)}$, and EP $^{(3)}$, respectively. Equation 1 can be rewritten in





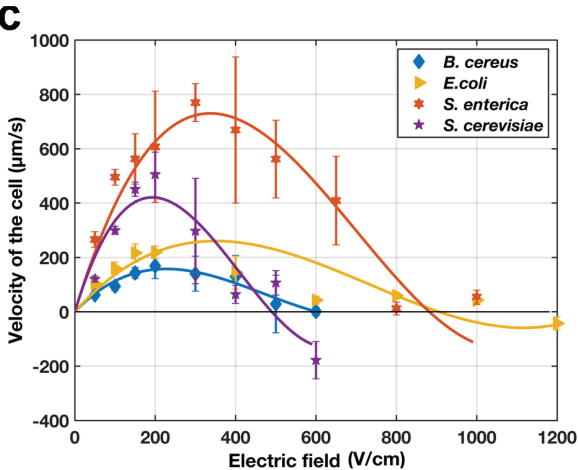


Figure 1. (a) Schematic of PIV channel representing negatively and positively charged particles under the effects of an electric potential difference. Arrows represent the direction of the predominant forces. In our system, EO flow direction is from left to right, while EP migration is from right to left. (b) Velocity of polystyrene particles as a function of the electric field. (c) Velocity of cells as a function of the electric field. Solid lines represent third order polynomial fits of the measured data. Data collection stopped when particle velocity reached approximately zero.

terms of the different mobilities, μ , related to these phenomena and the electric field, E, present in the microfluidic device:

$$\mathbf{v}_{\mathrm{P}} = \mu_{\mathrm{EO}} \mathbf{E} + \mu_{\mathrm{EP}}^{(1)} \mathbf{E} + \mu_{\mathrm{EP}}^{(3)} (\mathbf{E} \cdot \mathbf{E}) \mathbf{E}$$
 (2)

There are two important regimes to consider: At low electric fields, the linear EO and $EP^{(1)}$ phenomena dominate total

Table 1. Microparticle Information and EK Properties Determined in This Study

#	particle diameter (μm)	mfr.	surface funct.	low-voltage fitting eq.	charge (meq/g)	$\zeta_{ m P}~({ m mV})$	$\mu_{\rm EP}^{(1)} \times 10^{-8}$ (m ² V ⁻¹ s ⁻¹)	$E_{\rm EEC}$ (V/cm)	$\mu_{\rm EP}^{(3)} \times 10^{-19}$ (m ⁴ V ⁻³ s ⁻¹)
1	2.0	Inv	carboxyl	$y = 2.49x + 3.89$ $R^2 = 0.995$	0.065	-58 ± 5	-4.51 ± 0.36	481 ± 70.92	-42.15 ± 10
2	2.0	Mag	carboxyl	$y = 0.56x + 0.41$ $R^2 = 0.998$	0.006	-1 ± 2	-0.06 ± 0.16	2507 ± 50.60	-8.97 ± 0.36
3	5.1	Mag	nonfunct.	$y = 0.35x - 1.47$ $R^2 = 0.999$	NA	-28 ± 1	-2.16 ± 0.10	3722 ± 358.58	-2.46 ± 0.45
4	6.8	Mag	carboxyl	$y = 3.55x + 89.37$ $R^2 = 0.995$	0.013	-10 ± 8	-0.80 ± 0.59	2165 ± 191.50	-9.86 ± 2.36

^aInv: Invitrogen; Mag: Magsphere.

Table 2. Cell Strain Information and EK Properties Determined in This Study^a

cell strain	dimensions (µm)	low-voltage fitting eq	$\zeta_{ m P}~({ m mV})$	$\mu_{\rm EP}^{(1)} \times 10^{-8} ({\rm m}^2 {\rm V}^{-1} {\rm s}^{-1})$	$E_{\rm EEC}$ (V/cm)	$\mu_{\rm EP}^{(3)} \times 10^{-19}$ (m ⁴ V ⁻³ s ⁻¹)
B. cereus (Gram+) ATCC 14579	$L: 4.94 \pm 0.47$ $W: 1.32 \pm 0.13$	$y = 0.81x + 18.59$ $R^2 = 0.9842$	-58 ± 2	-4.53 ± 0.17	604 ± 74.74	-28.62 ± 11
E. coli (Gram+) ATCC 25922	$L: 2.01 \pm 0.42$ $W: 0.97 \pm 0.21$	$y = 1.13x + 47.01$ $R^2 = 1$	-49 ± 4	-3.87 ± 0.32	1100 ± 7.68	-14.11 ± 0.20
S. enterica (Gram-) TT9079	$L: 2.00 \pm 0.31$ $W: 0.97 \pm 0.11$	$y = 2.97x + 144.70$ $R^2 = 0.910$	-12 ± 10	-3.48 ± 0.53	804 ± 63.07	-72.21 ± 10.46
S. cerevisiae ATCC 9763	$D: 6.23 \pm 0.77$	$y = 3.30x - 40.03$ $R^2 = 0.998$	-35 ± 4	-1 ± 0.82	537 ± 3.10	-97.09 ± 1.12

^aL: length; W: width; D: diameter.

particle velocity, 23,24,27 while at high electric fields the nonlinear EP⁽³⁾ phenomenon becomes the dominant mechanism. The mobilities associated with the two linear phenomena depend on the zeta potential of the particle ($\zeta_{\rm P}$) and the channel wall ($\zeta_{\rm W}$), as well as on the fluid viscosity (η) and permittivity ($\varepsilon_{\rm m}$).

$$\mu_{\rm EO} = -\frac{\zeta_{\rm W} \varepsilon_{\rm m}}{\eta} \tag{3}$$

$$\mu_{\rm EP}^{(1)} = \frac{\zeta_{\rm P} \varepsilon_m}{\eta} \tag{4}$$

With the purpose of characterizing the microparticles and cells, the parameters $\mu_{\rm EO}$ and $\mu_{\rm ED}^{(1)}$ were estimated first following standard procedures, as reported elsewhere. ^{28,29} In addition to these attributes, which are key for the design of DC-iEK experiments, the novel recently defined parameter referred to as $E_{\rm EEC}$, (i.e., the electric field at which EP⁽³⁾, EOF drag, and EP⁽¹⁾ are balanced, resulting in ${\bf v}_{\rm P}=0$) was also measured. ^{17,23} This attribute allows extrapolating the expected applied voltages required to achieve the trapping of a particle or microorganism across different microfluidic DC-iEK devices. This applied voltage value is commonly referred as the "trapping voltage", which is a system-dependent parameter, while $E_{\rm EEC}$ is a system-independent parameter. ²³ Evaluating eq 2 for trapping and solving for $\mu_{\rm EP}^{(3)}$ yields

$$\mu_{\rm EP}^{(3)} = -\frac{(\mu_{\rm EP}^{(1)} + \mu_{\rm EO})}{E_{\rm EEC}^2} \tag{5}$$

EXPERIMENTAL SECTION

Microdevices. Microdevices were made from PDMS (Dow Corning, MI, U.S.A.) using standard soft lithography techniques. ^{30,31} The microchannels (Figure 1a) had a constant

cross section, a length of 10.16 mm, a height of 40 $\mu m,$ and a width of 880 $\mu m.$

Suspending Medium. The suspending media was a buffer solution of $\rm K_2HPO_4$ (Amresco, New York, NY) at a 0.2 mM concentration, with the addition of 0.05% (v/v) of Tween 20 (Amresco, New York, NY) to prevent particle sticking. This suspending medium had a conductivity of 41 $\mu\rm S/cm$ and a pH of 7.3, which produced a wall zeta potential ($\rm \zeta_W$) of $\rm -71.6~mV$ and $\rm \mu_{EO} = 5.58 \times 10^{-8}~m^2~V^{-1}~s^{-1}$ in the PDMS devices, as measured with current monitoring. 29

Particle and Cell Samples. Four types of polystyrene microparticles were used in this study and are listed in Table 1. Based on their size, microsphere suspensions were diluted into the suspending media with concentrations ranging from 1.5×10^5 to 5.7×10^6 particles/mL. Four types of cells were also studied in this work, three bacteria and one yeast strain, as listed in Table 2. All microorganisms were cultured and stained following standard procedures. The stained cells were then suspended in the suspending medium.

Equipment and Software. Conductivity and pH were measured with a conductivity meter Thermo Scientific Orion STAR A212, and a pH meter Thermo Scientific STAR A2116. Experiments were recorded in the form of videos with a Zeiss Axiovert 40 CFL inverted microscope (Carl Zeiss Microscopy, Thornwood, NY) and Leica DMi8 inverted microscope (Wetzlar, Germany). The *Sequencer* software was used to control the high voltage power supply (Model HVS6000D, LabSmith, Livermore, CA) and apply voltage sequences to the microchannels via platinum electrodes.

Experimental Procedure. Particle image velocimetry (PIV) was used to assess particle migration within the microchannel shown in Figure 1a. Each PIV experiment started by filling the microchannels (Figure 1a) with the suspending medium (0.2 mM $\rm K_2HPO_4$, 0.05% (v/v) Tween 20). To decrease pressure driven backflow during the experiments, large reservoirs (\sim 2 mL) were placed at the

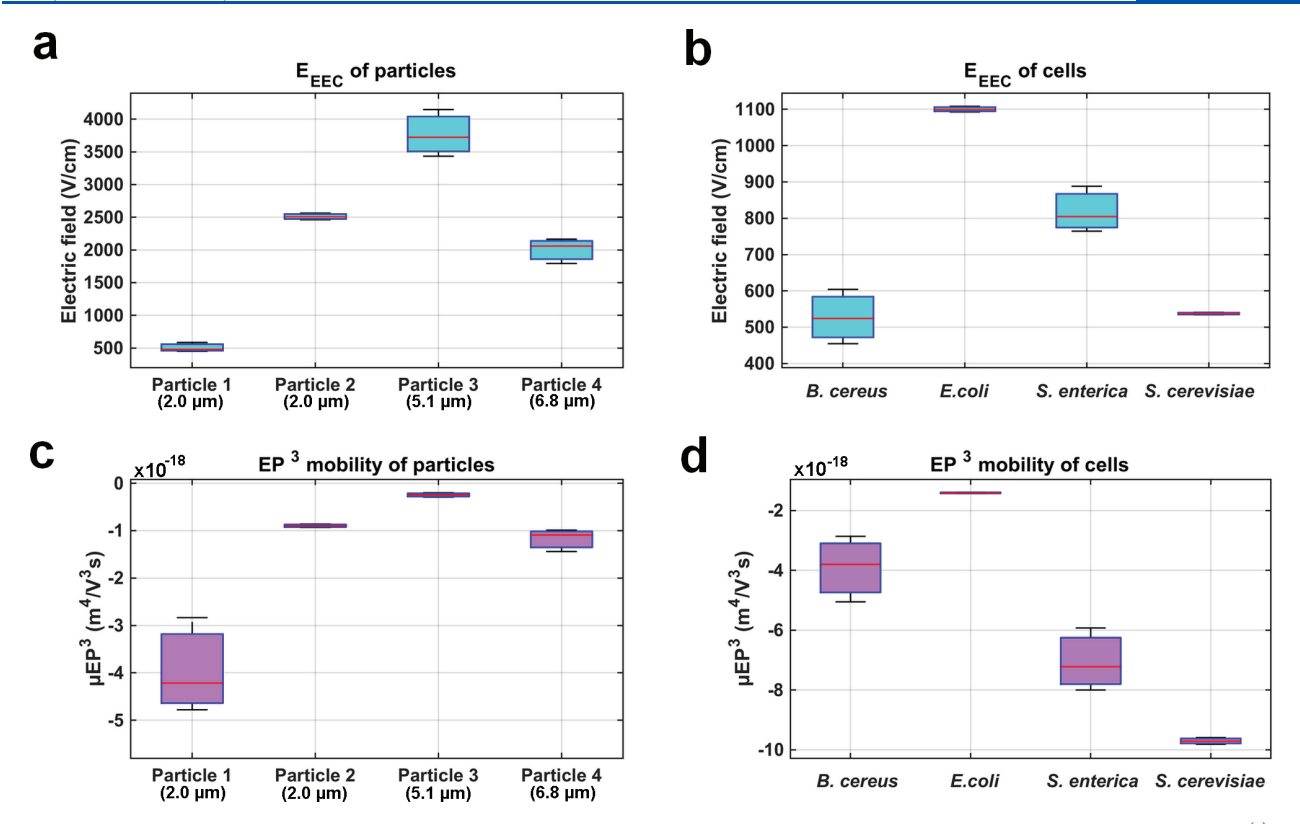


Figure 2. Boxplots representing estimated electrokinetic equilibrium condition ($E_{\rm EEC}$) and electrophoresis of the second kind mobility ($\mu_{\rm EP}^{(3)}$) of each particle and cell. (a) Boxplot of the $E_{\rm EEC}$ of the studied particles. (b) Boxplot of the $E_{\rm EEC}$ of cells. (c) Boxplot of the $\mu_{\rm EP}^{(3)}$ of particles. (d) Boxplot of the $\mu_{\rm EP}^{(3)}$ of cells.

inlet and outlet of the channel and were filled and leveled with the suspending medium. Sample suspensions $(3-8 \mu L)$ were introduced into the inlet reservoir, and platinum wire electrodes were also placed into the reservoirs. Particle and cell migration were observed and recorded at a range of applied voltages to observe both, linear and nonlinear, EK effects (Figure 1b,c). The range of applied voltages was customized for each sample to ensure the velocity profile for each particle or cell was properly characterized. Experiments were performed in triplicate. To keep data consistent, experiments stopped when the particles approximately reached their E_{EEC} . Also, because input voltage fidelity of the power supply lowers at higher voltages (and because trapping voltages were very high for some particles) exploring larger voltages would likely introduce noise to the system. We stress that the focus of this work was to determine the E_{EEC} of particles and cells; thus, we aimed at keeping the experiments suitable to determine $\mu_{\rm EP}^{(1)}$ and $\mu_{\rm EP}^{(3)}$ only.

The detailed voltage sequence applied for high voltage PIV experiments is included in the Supporting Information. Briefly, velocity measurements were taken at target high voltages. Precautions (the use of large reservoirs and a K₂HPO₄ solution as suspending medium) were taken to avoid possible changes in pH of the suspending medium inside the channel due to the effects of high voltages. *ImageJ* software was used for video analysis to estimate particle and cell velocities using particle image velocimetry (PIV).

RESULTS AND DISCUSSION

Low-Voltage PIV Measurements and Determination of Linear EK Parameters. A series of low-voltage (<200 V)

PIV measurements were carried out to estimate the linear EP mobility $(\mu_{\rm EP}^{(1)})$ of particles and cells, as well as their zeta potential $(\zeta_{\rm P})$. The detailed velocity data obtained under low voltage is listed in Table S1 (Supporting Information) and plotted in Figure 1b,c; this data was fitted to a straight line and the fitting equations are listed in Tables 1 and 2. Equation 2 was used (neglecting the $\mu_{\rm EP}^{(3)}$ term since low voltages were applied) to estimate $\mu_{\rm EP}^{(1)}$, since $\mu_{\rm EO}$ was known from current monitoring experiments. Particle and cell zeta potential values were directly estimated from $\mu_{\rm EP}^{(1)}$ values with eq 4 and are reported in Tables 1 and 2. It is important to note that particle and cell behavior must be strictly linear with the electric field for these measurements to be accurate (i.e. EP⁽³⁾ effects should be negligible); considering this, the maximum applied voltages for all of the measurements listed in Table S1 were between 150 and 200 V.

Low-voltage behavior on the four types of polystyrene particles, ruled by the linear effects of EO flow and EP⁽¹⁾ force, is represented by the first three velocity data points plotted in Figure 1b for each particle. Therefore, their linear electrophoretic mobilities ($\mu_{\rm EP}^{(1)}$) could be calculated directly from their velocities (Tables 1 and S1), ranging from -4.6×10^{-8} to -0.06×10^{-8} (m² V⁻¹ s⁻¹) with a maximum standard deviation of 0.54 \times 10⁻⁸ (m² V⁻¹ s⁻¹). The estimation of particle zeta potential values ($\zeta_{\rm P}$), which accounts for the ionic strength of the suspending medium, was taken directly from $\mu_{\rm EP}^{(1)}$ using eq 4, and the mean values varied from -1 to -58 mV.

Similar to velocity measurements of polystyrene particles, the first three data points plotted in Figure 1c represent the linear behavior of the four strains of microorganisms at low

electric fields. The accuracy of the linear fit equation for this data (shown in Tables 2 and S1) was high, having an R^2 parameter ranging from 0.91 to 1. As mentioned, at low electric fields, the linear increase in velocity in relation to the electric field is dominated by EO flow and the $EP^{(1)}$ force. In this study, all microorganisms had average $\mu_{\rm EP}^{(1)}$ values varying between -4.53×10^{-8} and -1×10^{-8} m 2 V $^{-1}$ s $^{-1}$. To determine the $\zeta_{\rm P}$ of the studied cells, eq 4 was used (considering EP $^{(3)}$ effects as negligible). This is a broadly accepted model to calculate the zeta potential values of bacteria and other types of microorgansims. Table 2 shows that *S. enterica*, *S. cerevisiae*, *E. coli*, and *B. cereus* had average zeta potential values of -12, -35, -49, and -58 mV, respectively.

As expected, the EK behavior of particles and cells stimulated with low voltages exhibited a linear response and the estimations were in excellent agreement with previously reported data in the literature.³² We emphasize that, according to the conventional "iDEP" theory, particle trapping (or particle flow reversal) could only be expected in channels with insulating posts and explained by DEP.³¹ In a straight channel, like the one presented herein, trapping would not be expected and could definitely not be explained. However, as observed in Figure 1b,c, the linear trend is not sustained as the electric field magnitude increases, and after reaching a maxima, velocity decreases and an eventual overall zero particle velocity can, in fact, be obtained as reported recently.¹⁷,23

High Voltage PIV Measurements and Determination of Nonlinear EK Parameters. After the low-voltage PIV measurements were done, particle and cell migration were also assessed, employing a series of high voltages (>200 V), following the experimental procedure detailed previously. For the analysis of these experiments, for each recorded video, the velocities obtained from PIV measurements were arranged in histograms set so that the highest bin represented a 20% of the velocity population. Then, the average velocity of each highest bin of the histograms was calculated. For each experiment, the average values of each repetition were averaged, and their standard deviation were calculated and plotted as a function of the applied electric field. Figure 1b,c shows the complete velocity curves of particles and microorganisms. These velocity curves clearly illustrate the nonlinear behavior due to the onset of EP⁽³⁾ effects at high electric fields. As it can be observed, the velocity continues decreasing until the microparticles and microorganisms eventually stop (on average), reaching their $E_{\rm EEC}$ at ${\bf v}_{\rm p}$ = 0, and as the electric field further increased the particles and cells even experienced negative velocities (i.e., their flow direction reversed).

To calculate the $E_{\rm EEC}$ of each particle and cell, interpolations or extrapolations were done using the two velocity data points closest to zero at high voltages. Interpolation estimations were done if those data points crossed the x-axis, and extrapolation estimations were done if they did not. Because of the abundance of data and the proximity between data points, linear interpolation/extrapolation was assumed. With the $E_{\rm EEC}$ results, the calculation of $\mu_{\rm EP}^{(3)}$ followed directly from evaluating eq 5. The $E_{\rm EEC}$ and $\mu_{\rm EP}^{(3)}$ parameters of each particle and cell type are shown in Figure 2, as well as in Tables 1 and 2.

As the electric field increased, the onset of $EP^{(3)}$ caused all studied polystyrene particles to experience a nonlinear velocity behavior (Figure 1b). Nonetheless, these behaviors are not necessarily similar since each particle has a distinct $\mu_{EP}^{(3)}$. The estimated values for $\mu_{EP}^{(3)}$ on the studied particles were in the

range between -2.46×10^{-19} and -42.15×10^{-19} (m⁴ V⁻³ s⁻¹), as shown in both Figure 2c and Table 1. As described earlier, due to $\mu_{\rm EP}^{(3)}$, the particles experience negative velocities at high electric fields and exhibit an equilibrium point, where the average velocity of the particle is zero (E_{EEC}) . As can be observed in Figure 2a and Table 1, where the $E_{\rm EEC}$ of each particle is shown, particle 1 reached its $E_{\rm EEC}$ at lower electric fields (481 \pm 70.92 V/cm) than the rest. One of the main reasons for this behavior may be found in its size $(2 \mu m)$, as it is the smallest from the pack. In addition, it has the greatest zeta potential (-59 \pm 4 mV) and $\mu_{EP}^{(3)}$ (-42.15 \times 10⁻¹⁹ m⁴ V⁻³ s⁻¹). The large $\mu_{\rm EP}^{(3)}$ is translated as a stronger force pointing toward the inlet of the channel, forcing the particle to move backward (Figure 1a). In contrast, particle 3 had the lowest $\mu_{\rm EP}^{(3)}$ value $(-2.46 \times 10^{-19} \, {\rm m}^4 \, {\rm V}^{-3} \, {\rm s}^{-1})$, allowing the particle to reach the highest velocity and preventing it from reaching a negative average velocity in our experiments. For this reason, its estimated $E_{\rm EEC}$ (3722 V/cm) had the greatest standard deviation (358.58 V/cm). Particles 2 and 4 reached their $E_{\rm EEC}$ at 2507 and 2165 V/cm, and had a $\mu_{\rm EP}^{(3)}$ of -8.97×10^{-19} and $-9.86 \times 10^{-19} \text{ (m}^4 \text{ V}^{-3} \text{ s}^{-1})$, respectively.

As can be observed in both Figure 2b and Table 2, each cell strain studied also reached its $E_{\rm EEC}$ at different electric fields and exhibited an error ranging from 1 to 12%. It is important to notice that even with E. coli and S. enterica having a very similar morphology, they reached their E_{EEC} at very different electric fields (1100 and 804 V/cm, respectively). In contrast to polystyrene particles, where the smallest one (particle 1) with the highest zeta potential reached its E_{EEC} at very low electric fields, E. coli, which has one of the smallest dimensions of the studied cells and the second higher zeta potential (-49 mV), had the smallest $\mu_{\rm EP}^{(3)}$ (-14.11 \pm 0.20 \times 10⁻¹⁹ m⁴ V⁻³ s^{-1}) and, therefore, the highest E_{EEC} . S. cerevisiae reached the lower $E_{\rm EEC}$ value (537 V/cm) and had the largest $\mu_{\rm EP}^{(3)}$ (-97.09 $\pm 1.12 \times 10^{-19} \text{ m}^4 \text{ V}^{-3} \text{ s}^{-1}$). *B. cereus* experienced $\mu_{\text{EP}}^{(3)}$ values of $-28.62 \pm 11 \times 10^{-19} \text{ (m}^4 \text{ V}^{-3} \text{ s}^{-1)}$, which due to its shape, can have a higher population distribution, which can lead to an increased standard deviation in the results. It is important to note that, as expected, a clear correlation exists between particles' charge density and their measured zeta potential. This can be verified in Table 1, which illustrates that the larger the magnitude of the particle charge density (reported as meq/ g), the greater the magnitude of the particle zeta potential. Nonetheless, although nonlinear EK phenomena depend on particle size and charge density, a clear trend could not be observed between these properties in our system and the observed nonlinear EK response of the particles. These results reveal that new DC-iEK experiments must be designed to further isolate linear and nonlinear phenomena and unveil the currently hidden relationship between physical properties and the EK cell responses here presented.

This is a pioneering report of experimentally characterized nonlinear electrophoretic mobilities $(\mu_{\rm EP}^{(3)})$ of polystyrene particles, prokaryote bacterial cells, and eukaryote yeast cells. Furthermore, the present study also characterized the electrokinetic equilibrium conditions $(E_{\rm EEC})^{17,23,24}$ for all particles and cells tested. The linear and nonlinear EK parameters reported here for polystyrene particles and cells, together with those recently reported by Tottori et al. for submicron (polystyrene and PMMA) particles, which are in good agreement with our measurements for polystyrene microparticles, add to the growing body of literature that highlights the importance of nonlinear EK phenomena in particle

trapping applications. Furthermore, they will allow for the design of novel DC-iEK systems that can be tailored for challenging separations. The introduction of the nonlinear phenomenon of EP of the second kind represents a major change in our understanding of particle migration in DC-iEK devices. Moreover, the use of these linear and nonlinear EK parameters ensure that modeling results better represent reality, enabling accurate predictions of particle migration in DC-iEK devices and removing the previous requirement of introducing correction factors²⁶ into inadequate models.

ASSOCIATED CONTENT

Supporting Information

The Supporting Information is available free of charge at https://pubs.acs.org/doi/10.1021/acs.analchem.0c03525.

The detailed procedure followed for high-voltage PIV experiments, as well as Table S1, listing the detailed data obtained with low-voltage PIV for polystyrene particles and cells (PDF)

AUTHOR INFORMATION

Corresponding Authors

Victor H. Perez-Gonzalez — School of Engineering and Sciences, Tecnologico de Monterrey, Monterrey, NL 64849, Mexico; orcid.org/0000-0003-4503-7774; Email: vhpg@tec.mx

Blanca H. Lapizco-Encinas — Microscale Bioseparations Laboratory and Biomedical Engineering Department, Rochester Institute of Technology, Rochester, New York 14623, United States; orcid.org/0000-0001-6283-8210; Email: bhlbme@rit.edu

Authors

Sofia Antunez-Vela — Microscale Bioseparations Laboratory and Biomedical Engineering Department, Rochester Institute of Technology, Rochester, New York 14623, United States; School of Engineering and Sciences, Tecnologico de Monterrey, Monterrey, NL 64849, Mexico

Adriana Coll De Peña — Microscale Bioseparations Laboratory and Biomedical Engineering Department, Rochester Institute of Technology, Rochester, New York 14623, United States; Thomas H. Gosnell School of Life Sciences, Rochester Institute of Technology Rochester, Rochester, New York 14623, United States

Cody J. Lentz – Microscale Bioseparations Laboratory and Biomedical Engineering Department, Rochester Institute of Technology, Rochester, New York 14623, United States

 $Complete\ contact\ information\ is\ available\ at: \\ https://pubs.acs.org/10.1021/acs.analchem.0c03525$

Author Contributions

S.A.V.: Methodology, experimentation, cell culture, data analysis, writing original draft: review and editing. V.H.P.G.: Conceptualization, supervision, data analysis, writing original draft: review and editing. A.C.D.P.: Methodology, experimentation, cell culture, writing original draft — review and editing. C.J.L.: Methodology, experimentation, review and editing. B.H.L.E.: Conceptualization, project administration, supervision, writing original draft: review and editing.

Notes

The authors declare no competing financial interest.

ACKNOWLEDGMENTS

The authors would like to acknowledge the financial support provided by the National Science Foundation (Award CBET-1705895). This work was also financially supported by the Nano-Sensors and Devices Research Group of Tecnologico de Monterrey (0020240I03).

REFERENCES

- (1) Hölzel, R.; Pethig, R. Micromachines 2020, 11 (5), 533.
- (2) Lapizco-Encinas, B. H. Curr. Opin. Chem. Eng. 2020, 29, 9-16.
- (3) Lapizco-Encinas, B. H. Electrophoresis 2019, 40 (3), 358-375.
- (4) Keck, D.; Stuart, C.; Duncan, J.; Gullette, E.; Martinez-Duarte, R. Micromachines 2020, 11 (6), 625.
- (5) Crowther, C. V.; Hilton, S. H.; Kemp, L. K.; Hayes, M. A. Anal. Chim. Acta 2019, 1068, 41–51.
- (6) Coll De Peña, A.; Mohd Redzuan, N. H.; Abajorga, M.; Hill, N.; Thomas, J. A.; Lapizco-Encinas, B. H. *Micromachines* **2019**, *10* (7), 450
- (7) Kim, D.; Sonker, M.; Ros, A. Anal. Chem. 2019, 91 (1), 277–295.
- (8) Fernandez, R. E.; Rohani, A.; Farmehini, V.; Swami, N. S. *Anal. Chim. Acta* **2017**, *966*, 11–33.
- (9) Holzel, R.; Calander, N.; Chiragwandi, Z.; Willander, M.; Bier, F. F. *Phys. Rev. Lett.* **2005**, 95 (12), 128102.1–128102.4.
- (10) Fazelkhah, A.; Afshar, S.; Durham, N.; Butler, M.; Salimi, E.; Bridges, G.; Thomson, D. *Electrophoresis* **2020**, *41* (9), 720–728.
- (11) McGrath, J. S.; Honrado, C.; Spencer, D.; Horton, B.; Bridle, H. L.; Morgan, H. Sci. Rep. **2017**, 7 (1), na DOI: 10.1038/s41598-017-02715-y.
- (12) Zhang, Y.; Wang, S.; Chen, J.; Yang, F.; Li, G. BioChip J. 2020, 14 (2), 185–194.
- (13) Jung, W.; Han, J.; Choi, J.-W. W.; Ahn, C. H. Microelectron. Eng. **2015**, 132, 46–57.
- (14) Adekanmbi, E. O.; Srivastava, S. K. Lab Chip **2016**, 16 (12), 2148–2167.
- (15) Xuan, X. Electrophoresis 2019, 40 (18-19), 2484-2513.
- (16) Rohani, A.; Moore, J. H.; Kashatus, J. A.; Sesaki, H.; Kashatus, D. F.; Swami, N. S. *Anal. Chem.* **2017**, 89 (11), 5757–5764.
- (17) Cardenas-Benitez, B.; Jind, B.; Gallo-Villanueva, R. C.; Martinez-Chapa, S. O.; Lapizco-Encinas, B. H.; Perez-Gonzalez, V. H. *Anal. Chem.* **2020**, *92* (19), 12871–12879.
- (18) Shilov, V.; Barany, S.; Grosse, C.; Shramko, O. Adv. Colloid Interface Sci. **2003**, 104 (1–3), 159–173.
- (19) Dukhin, S. S. Adv. Colloid Interface Sci. 1991, 35 (C), 173-196.
- (20) Rouhi Youssefi, M.; Diez, F. J. Electrophoresis 2016, 37 (5-6), 692-698.
- (21) Tottori, S.; Misiunas, K.; Keyser, U. F.; Bonthuis, D. J. Phys. Rev. Lett. 2019, 123 (1), 14502.
- (22) Kumar, A.; Elele, E.; Yeksel, M.; Khusid, B.; Qiu, Z.; Acrivos, A. *Phys. Fluids* **2006**, *18* (12), 1–11.
- (23) Coll De Peña, A.; Miller, A.; Lentz, C. J.; Hill, N.; Parthasarathy, A.; Hudson, A. O.; Lapizco-Encinas, B. H. *Anal. Bioanal. Chem.* **2020**, 412 (16), 3935–3945.
- (24) Coll De Peña, A.; Hill, N.; Lapizco-Encinas, B. H. Biosensors 2020, 10 (10), 148.
- (25) Quevedo, D. F; Lentz, C. J; Coll de Pena, A.; Hernandez, Y.; Habibi, N.; Miki, R.; Lahann, J.; Lapizco-Encinas, B. H *Beilstein J. Nanotechnol.* **2020**, *11*, 1556–1567.
- (26) Hill, N.; Lapizco-Encinas, B. H. Electrophoresis 2019, 40 (18–19), 2541–2552.
- (27) Ayala-Mar, S.; Perez-Gonzalez, V. H.; Mata-Gómez, M. A.; Gallo-Villanueva, R. C.; Gonzalez-Valdez, J. Anal. Chem. 2019, 91 (23), 14975–14982.
- (28) Hidalgo-Caballero, S.; Lentz, C. J.; Lapizco-Encinas, B. H. *Electrophoresis* **2019**, 40 (10), 1395–1399.
- (29) Saucedo-Espinosa, M. A.; Lapizco-Encinas, B. H. Biomicrofluidics 2016, 10 (3), 033104.

- (30) Duffy, D. C.; McDonald, J. C.; Schueller, O. J. A.; Whitesides,
- G. M. Anal. Chem. **1998**, 70 (23), 4974–4984. (31) Saucedo-Espinosa, M.A.; Lapizco-Encinas, B.H. J. Chromatogr. A **2015**, 1422, 325–333.
- (32) Polaczyk, A. L.; Amburgey, J. E.; Alansari, A.; Poler, J. C.; Propato, M.; Hill, V. R. *Colloids Surf., A* **2020**, 586, 124097.